Characterization of the molecular properties of KtrC, a second RCK domain that regulates a Ktr channel in *Bacillus subtilis*

Rita Rocha[a,b], Celso M. Teixeira-Duarte[a,b,c], João M. P. Jorge[a,b], João Henrique Morais-Cabral[a,b,*]

[a] i3S - Instituto de Investigação e Inovação em Saúde, Universidade do Porto

[b] IBMC - Instituto de Biologia Molecular e Celular, Universidade do Porto, Porto, Portugal.

[c] Programa Doutoral em Biologia Molecular e Celular (MCbiology), Instituto de Ciências Biomédicas Abel Salazar (ICBAS), Universidade do Porto, Porto, Portugal

[*] Corresponding author: jcabral@ibmc.up.pt (JH Morais-Cabral)

Abstract

RCK (regulating conductance of K^+) domains are common regulatory domains that control the activity of eukaryotic and prokaryotic K^+ channels and transporters. In bacteria these domains play roles in osmoregulation, regulation of turgor and membrane potential and in pH homeostasis. Whole-genome sequencing unveiled RCK gene redundancy, however the biological role of this redundancy is not well understood. In *Bacillus subtilis*, there are two closely related RCK domain proteins (KtrA and KtrC) that regulate the activity of the Ktr cation channels. KtrA has been well characterized but little is known about KtrC. We have characterized the structural and biochemical proprieties of KtrC and conclude that KtrC binds ATP and ADP, just like KtrA. However, in solution KtrC exist in a dynamic equilibrium between octamers and non-octameric species that is dependent on the bound ligand, with ATP destabilizing the octameric ring relative to ADP. Accordingly, KtrC-ADP crystal structures reveal closed octameric rings similar to those in KtrA, while KtrC-ATP adopts an open assembly with RCK domains forming a super-helix. In addition, both KtrC-ATP and -ADP octamers are stabilized by the signaling molecule cyclic-di-AMP, which binds to KtrC with high affinity. In contrast, c-di-AMP binds with 100-fold lower affinity to KtrA. Despite these differences we show with an *E. coli* complementation assay that KtrC and KtrA are interchangeable and able to form functional transporters with both KtrB and KtrD. The distinctive properties of KtrC, in particular ligand-dependent assembly/disassembly, suggest that this protein has a specific physiological role that is distinct from KtrA.

Highlights

- KtrC adopts different oligomeric states in solution.
- KtrC-ADP structures shows octameric rings that resemble KtrA.
- KtrC-ATP structure shows an “open” or disrupted octameric ring.
- KtrC and KtrA are functionally redundant in an *E. coli* complementation assay.
- Cyclic-di-AMP binds to KtrC with high-affinity, stabilizing KtrC octamers.

Keywords

RCK domain, crystal structure, ion channels, ligand-dependent oligomerization, cyclic-di-AMP

Introduction

RCK (regulator of conductance of K^+) domains are widespread regulatory domains of K^+ channels and transporters. These domains are dimeric or pseudo-dimeric ligand binding proteins that commonly assemble into a ring structure with four dimers (Albright et al., 2006; Cao et al., 2013; Dong et al., 2005; Jiang et al., 2001; Jiang et al., 2002; Roosild et al., 2002; Roosild et al., 2009; Vieira-Pires et al., 2013; Ye et al., 2006). Upon ligand binding the conformation of the RCK dimeric unit is altered, resulting in the rearrangement of the ring and leading to activation of the effector membrane protein, the channel or transporter (Cao et al., 2013; Diskowski et al., 2017; Szollosi et al., 2016; Vieira-Pires et al., 2013).

RCK domains regulate the activity of eukaryotic Slo K^+ channels and structural studies have revealed the mechanisms of channel activation (Hite and MacKinnon, 2017; Hite et al., 2015; Leonetti et al., 2012; Wu et al., 2010; Yuan et al., 2010). RCK domains are also common in prokaryotic K^+ channels and transporters with key roles in osmoregulation, pH homeostasis, regulation of turgor pressure and membrane potential (Bakker and Mangerich, 1981; Epstein and Schultz, 1965; Kroll and Booth, 1981; Meury et al., 1985; Whatmore and Reed, 1990). Structures of several prokaryotic channels regulated by RCK domains have been determined. Among them are the GsuK (Kong et al., 2012) and MthK (Jiang et al., 2002) K^+ channels and the cation channels TrkHA (Cao et al., 2013) and KtrAB (Diskowski et al., 2017; Szollosi et al., 2016; Vieira-Pires et al., 2013).

The KtrAB protein complex from *Bacillus subtilis* belongs to the family of Ktr cation channels that are essential components of the K^+ homeostasis machinery in some bacteria (Corratge-Faillie et al., 2010; Diskowski et al., 2015; Levin and Zhou, 2014). In *Staphylococcus aureus*, a single RCK domain protein appears to regulate two Ktr

membrane proteins, suggesting a single mode of control of the activity of these channels (Grundling, 2013; Price-Whelan et al., 2013). In contrast, many other bacterial genomes reveal the presence of multiple RCK domain proteins with closely related amino acid sequences. *Bacillus subtilis* has two membrane protein genes, KtrB and KtrD, and two regulatory subunit RCK domain genes, KtrA and KtrC (Holtmann et al., 2003). The genes for KtrA and KtrB are organized in an operon; a homodimer of the membrane protein KtrB assembles with the cytoplasmic KtrA octameric ring giving rise to the KtrAB complex (Vieira-Pires et al., 2013). KtrA binds nucleotides, ATP or ADP, and crystal structures of the isolated KtrA octameric ring or of the KtrAB complex have revealed different octameric ring conformations that are dependent on the bound ligand (Szollosi et al., 2016; Vieira-Pires et al., 2013). In contrast, much less is known about KtrC and KtrD. These two genes are positioned in different regions of the genome. KtrC is 53% identical to KtrA (Figure S1) and it has been proposed that KtrC and KtrD associate and form the KtrCD complex. It has been reported that KtrAB has a primary role in the mechanism of osmotic adaptation and that KtrCD is a less efficient K^+ uptake complex (Holtmann et al., 2003).

To better understand the roles of closely related RCK domains in bacteria and in particular, to better understand the regulatory network of the K^+ transport proteins in *B. subtilis*, we characterized the molecular properties of the KtrC RCK domain and compared them with the properties of KtrA. This characterization provides insights into the role of KtrC in the bacterial cell and lays the basis to understand the overall regulation of the bacterial K^+ homeostasis machinery.

Material and Methods

Protein expression and purification

B. subtilis KtrC was cloned into pET-24a (Novagen) without a fused affinity-purification tag. Transformed *Escherichia coli* BL21 (DE3) were grown in LB media supplemented with 50 µg/ml kanamycin until A_{600} = 0.5-0.6. KtrC expression was induced with 0.5 mM IPTG after immersion of the growth culture on ice for 30 min and addition of 1% (v/v) ethanol. Induction continued for 14-16 hours at 20°C. Cell pellet was resuspended in Buffer A [50 mM Tris-HCl pH 7.5, 150 mM KCl, 5 mM DTT], supplemented with protease inhibitors immediately before lysis. Cell lysate was cleared by centrifugation (34,957 *x g* for 45 min at 4°C) and then loaded into an anion-exchange column. KtrC was eluted with a 50-1000 mM KCl gradient. Fractions containing KtrC were incubated overnight with ATP-agarose beads (Jena Bioscences) at 4°C. Beads were extensively washed by gravity-flow with Buffer B [50 mM Tris-HCl pH 8.0, 150 mM KCl, 5 mM DTT] and protein was eluted with 5 mM ATP or ADP in Buffer B. Purified KtrC was concentrated to 10 mg/ml.

B. subtillis KtrD was cloned into pRSFDuet-1 (Novagen) and N-terminal His-tagged KtrD was overexpressed in *Escherichia coli* BL21 (DE3) grown in LB media supplemented with kanamycin 50 µg/ml. KtrD expression was induced at late-exponential phase with 0.5 mM IPTG during 2 hours at 37°C, in the presence of 1 mM $BaCl_2$. Bacterial cells were lysed in Buffer C [50 mM Tris-HCl pH 8.0, 120 mM NaCl, 30 mM KCl] supplemented with protease inhibitors and KtrD was extracted overnight at 4°C with 40 mM DDM (n-Dodecyl-β-D-Maltopyranoside). Cell lysate was cleared by centrifugation (34,957 *x g* for 45 min at 4°C) and subsequently split, with one half incubated with 2 mg purified KtrC-ATP during 1 hour at 4°C with gentle agitation. 5 mM Imidazole was added to the cell lysates. Cell lysates were loaded into a 375 µl Co^{2+}

resin (Talon) column pre-equilibrated with Buffer D [50 mM Tris-HCl pH 8.0, 120 mM NaCl, 30 mM KCl, 1 mM DDM] supplemented with 5 mM Imidazole. Co^{2+} resin was washed with ten column volumes, firstly with Buffer D supplemented with 5 mM Imidazole and next with Buffer D + 20 mM Imidazole. KtrD and KtrCD were eluted with Buffer D supplemented with 150 mM Imidazole and immediately diluted three times in Buffer D with 15 mM DTT. KtrD and KtrCD were dialyzed overnight at 4°C against Buffer E [50 mM Tris-HCl pH 8.0, 120 mM NaCl, 30 mM KCl, 1 mM DDM, 5 mM DTT]. Dialyzed protein was concentrated to ~ 1 mg/ml and analyzed by size exclusion chromatography.

Crystallization

All KtrC crystals grew at 20°C by sitting-drop vapor-diffusion method (Swissci 48-well plates), by mixing 1 µl of protein and 1 µl crystallization solution.

KtrC-ATP-Ca^{2+} were obtained by crystallization of KtrC-ATP in the presence of $CaCl_2$; prior to crystallization protein was purified by size-exclusion in buffer B and 1 mM ATP and 1 mM $CaCl_2$ were added to the pooled fractions. Protein was concentrated to 5 mg/ml. Crystals grew with 17-22% (v/v) 1,4-butanediol, 150-225 mM NaCl, 100 mM HEPES-Na (pH 7.5). Before being flash-cooled in liquid nitrogen, KtrC-ATP-Ca^{2+} crystals were soaked for 10-15 seconds in crystallization solution containing 5% (v/v) ethylene glycol.

KtrC-ATP crystals grew in crystallization conditions from the Morpheus screen (Molecular dimensions): 20-30% Ethylene glycol/PEG8000 (2:1), 100 mM Sodium HEPES/MOPS pH 7.5, 90-110 mM $NaNO_3/Na_2HPO_4/(NH_4)_2SO_4$ (1:1:1); protein was

directly eluted from ATP-agarose beads and concentrated to 6-8 mg/ml. Crystals were directly flashed-cooled in liquid nitrogen without additional cryoprotectant.

KtrC-ADP used for crystallization came directly from ATP-agarose beads, eluted with 5 mM ADP and concentrated to 6-8 mg/ml. KtrC-ADP crystals were obtained in 3.25-3.75 M Sodium Formate (pH 7.5) or in 0.7-1.0 M NaH_2PO_4, 1.4 M K_2HPO_4, 100 mM NaAcetate pH 4.5. In the first crystallization condition, crystals were transferred to 4.5 M Sodium Formate (pH 7.5) before flash-cooling. In the second crystallization condition, mother liquor supplemented with 1 mM ADP and 8% glycerol was used as cryosolution.

Data processing and structure determination

Diffraction data were collected at the Soleil synchrotron and were integrated and scaled with XDS and analyzed by AIMLESS (CCP4 package) (Winn et al., 2011). The KtrC-ATP-Ca^{2+} structure was determined by molecular replacement with Phaser (CCP4 package) using two models: N-terminal domain of KtrA-ATP (residues 6 to 124 of monomer A and 124 to 138 of monomer B; PDB accession number 4J90), and its C-terminal domain (140-217 of monomer B; PDB accession number 4J90). The final model was obtained by rounds of manual model building in COOT and refinement in Phenix (Adams et al., 2002) with three TLS groups (residues 2-120; 121-134; and 135-217).

Molecular replacement solutions for the low resolution diffraction datasets were obtained with Phaser (CCP4 package) using a collection of KtrA structures deposited in the PDB database. N- and C-terminal domains of the refined KtrC-ATP-Ca^{2+} structure were subsequently superimposed on the correspondent regions of the molecular

replacement solutions and the models were refined by rigid-body using Phenix. In order to validate the refinement applied to the model, Phaser runs were repeated using the original molecular replacement solution, the model with the KtrC lobes placed but before rigid body refinement and the final model after rigid body refinement. The highest Log of Likelihood score was obtained for the refined structural model indicating the improved agreement with diffraction data after refinement steps.

KtrC ligand binding

KtrC ligand binding proprieties were evaluated as before for *B. subtilis* (Vieira-Pires et al., 2013). KtrC bound to ADP-agarose was incubated for 30 min in 50 mM Tris-HCl pH 8.0, 150 mM KCl, 5 mM DTT with 1, 5 and 10 mM of different ligands: ATP, ADP, AMP, NAD^+, NADH, FAD and buffer without ligand as negative control. Eluted fractions were analyzed by SDS–PAGE.

Oligomeric analysis by size-exclusion chromatography

Analytical size exclusion chromatography was performed using a Superdex 200 10/300 GL column (GE Healthcare). For each analysis, 500 µl of KtrC at 10, 6 and 3 mg/ml in the presence of 5 mM ATP or ADP and 5 mM $MgCl_2$ were loaded into the column equilibrated with 50 mM Tris-HCl pH 8.0, 150 mM KCl, 5 mM DTT, 0.5 mM $MgCl_2$, at a flow rate of 0.5 ml/min. Size-exclusion runs were also performed in the absence of $MgCl_2$ either in the protein sample or elution buffer. *Bacillus subtilis* KtrA (199 kDa), yeast alcohol dehydrogenase (147 kDa; Sigma), chicken egg white Conalbumin (75 kDa) and hen egg Ovalbumin (43 kDa; both from GE Healthcare) were used as molecular weight standards for gel filtration calibration

KtrC-ATP-Mg^{2+} and KtrC-ADP-Mg^{2+} (8 mg/ml) were incubated with 0.2 mM c-di-AMP. Complex formation was analyzed by size exclusion chromatography. For this, 50 µL of protein sample (400 µg) were injected in a Superdex 200 10/300 column (GE Healthcare) equilibrated with 50 mM Tris-HCl pH 8.0, 150 mM KCl, 5 mM DTT.

Complementation assay

The complementation assay in *Escherichia coli* TK2420 strain was performed as previously described for KtrAB transporter (Albright et al., 2007; Vieira-Pires et al., 2013). Accordingly, *B. subtilis* KtrC, KtrA, KtrB and KtrD were cloned into a constitutive bicistronic expression vector where each membrane protein was paired with a different RCK domain protein and transformed into TK24020; bacteria expressing each subunit alone were used as controls. Complementation was tested at different external K^+ concentrations by growing overnight pre-cultures in minimal growth medium [8 mM $(NH_4)_2S0_4$, 400 µM $MgSO_4$, 6 µM $FeSO_4$, 6 µM ferric chloride, 1 mM sodium citrate, 1 mg/l thiamine HCl, 2 g/l glucose, 10 mg/l $CaCl_2$, 69 mM phosphate buffer and 115 mM (K^+ + Na^+)] containing 30 mM K^+, performing a 1:1000 dilution into the minimal growth media containing 0.03, 0.1, 0.3, 1, 2, 6, 10, 30 or 115 mM and growing for 16 h at 37 °C. Cell density was measured at 595 nm.

Thermal shift assay

Thermal shift assays were performed in the iQ5 Real Time Detection System (Bio-Rad) using 96 well PCR plates, as described before (Harley et al., 2012). Briefly, 3 µM of KtrC-ADP in Buffer B were mixed with Sypro Orange Dye (5,000 x diluted; Sigma) and ligand (c-di-AMP, c-AMP, c-di-GMP and c-di-IMP) at 200 µM or 3 µM of KtrA-

ADP in 50 mM Tris-HCl pH 7.5, 150 mM KCl, 5 mM DTT were mixed with Sypro Orange Dye (5,000 x diluted; Sigma) and ligand (c-di-AMP, c-AMP, c-di-GMP and c-di-IMP) at 250 µM. The temperature at the minimum of the derivative of the fluorescence intensity curve was defined as melting temperature (T_m).

Isothermal Titration Calorimetry

KtrC-ADP was dialyzed overnight at 4 °C against 50 mM HEPES-Na (pH 8.0), 150 mM KCl, 5 mM $MgCl_2$, 1 mM TCEP, 0.5 mM ADP. KtrA-ADP was dialyzed overnight at 4 ºC against 50 mM HEPES-Na (pH 7.5), 150 mM KCl, 5 mM $MgCl_2$, 1 mM TCEP, 0.5 mM ADP. Isothermal Titration Calorimetry experiments were performed in a VP-ITC instrument (MicroCal) at 25°C. KtrC-ADP at 10 µM was titrated with 72 µM c-di-AMP by injecting 5x6 µl, 5x8 µl and 18x10 µl of the ligand into the cell and KtrA-ADP at 30 µM was titrated with 400 µM c-di-AMP by injecting 5x8 µl and 24x10 µl of the ligand into the cell.

Three to four independent experiments were performed for each protein. Data were analyzed with the AFFINImeter software package using a global fit protocol of the independent measurements (Dumas et al., 2016).

Deposition of coordinates and diffraction data

Diffraction data and refined coordinates for KtrC-ATP-Ca^{2+} structure have been deposited at the Protein Data Bank with code 6I8V.

Results

KtrC binds ATP and ADP

To characterize the ligand binding properties of *B. subtilis* KtrC we made use of the fact that this protein binds to ADP-agarose beads just like KtrA (Vieira-Pires et al., 2013). Bound KtrC was then eluted with different adenosine-containing ligands at 3 different concentrations. Our data shows that KtrC is easily eluted by ATP at 1 mM and increasing concentrations of the ligand do not increase the amount of eluted protein (Figure 1A). ADP appears slightly less efficient in elution, as less protein is eluted with 1 mM ADP than with 5 or 10 mM. In contrast, 10 mM of other nucleotides (AMP, NAD^+, NADH or FAD) are not sufficient to elute all the protein associated with the beads (cf. elution with ATP and other nucleotides, Figure 1A). As for KtrA, attempts to remove nucleotide ligand from KtrC resulted in protein precipitation, suggesting that the ligand has a structural role and making quantification of ligand affinity a challenging task. In any case, our qualitative analysis strongly indicates a preference of KtrC for ATP and ADP, mirroring what was previously observed for *B. subtilis* KtrA (Vieira-Pires et al., 2013) and suggesting that ATP and ADP are biologically relevant ligands that regulate KtrC function in the cell.

The oligomeric state of purified KtrC-ATP and -ADP was evaluated by size-exclusion chromatography. We loaded the same volume of sample (0.5 ml) at three different KtrC concentrations (10, 6 and 3 mg/ml) in the presence of 5 mM ATP or ADP and 5 mM $MgCl_2$; the divalent cation was included because it commonly closely associates with ATP and ADP in the cell. At 3 mg/ml, the elution traces show two elution peaks, the most pronounced at 13.9 ml elution volume and a less intense peak at 11.3 ml (Figure 1B). With increasing protein concentration, a shift is observed where the 11.3 ml peak becomes more pronounced relative to the peak at ~14 ml (Figure 1B). The KtrC subunit

has ~24 kDa molecular weight. Comparison with KtrA, that elutes at 11.4 ml and was previously shown to be an octamer in solution (Albright et al., 2006; Vieira-Pires et al., 2013), and with other molecular weight standard proteins, leads us to conclude that the 11.3 ml KtrC peak most likely corresponds to an octamer. The peak at 13.9 ml is likely to correspond to a tetramer, if we assume that the building block is the dimeric unit. These experiments strongly suggest that KtrC exists in dynamic equilibrium between different oligomeric species and that only at high protein concentrations is the octamer prevalent. In addition, comparison of the elution profiles of the ADP- and ATP-bound KtrC shows that at all protein concentrations the elution profile with ADP is shifted towards the higher molecular weight species, suggesting a shift of the equilibrium towards the octameric assembly and stabilization of the octamer by ADP.

Interestingly, Mg^{2+} appears to affect the distribution of the protein in the elution profile. Although the peaks in the absence of Mg^{2+} are broader, the elution profiles of KtrC-ATP at 6 and 3 mg/ml in the absence of Mg^{2+}show a single peak between13 and 14 ml (Figure 1C), while two peaks are observed in the presence of Mg^{2+}. This effect is not observed with KtrC-ADP, where even at 3 mg/ml it is possible to detect a small peak at ~14 ml, despite the broadening of the higher elution volume peak. These observations suggest that Mg^{2+} stabilizes the octameric species and that this effect is dependent on the bound ATP.

Crystal structures of KtrC-ADP and KtrC-ATP

In order to elucidate the molecular details underlying the oligomeric organization of *B. subtilis* KtrC, we solved crystal structures for the ADP- and ATP- bound states by

molecular replacement using a library of KtrA structures, including full octameric rings and parts of the ring, dimers and tetramers, with the N- and C-lobes separated (Table 1).

Two KtrC-ADP structures were determined at low-resolution (6.28 and 5.69 Å) (Figure 2A and 2B). Both crystal forms show the presence of an octameric ring that closely resembles the KtrA ring. The distances separating Asp34 (Cα) residues in opposite ring subunits are 35/29 Å and 31/28 Å for the two structures, showing that the rings with ADP adopt a non-square conformation, which in KtrA corresponds to a low-activity or non-active conformation (Szollosi et al., 2016; Vieira-Pires et al., 2013). Two crystal structures were solved for KtrC-ATP, one at low resolution (4.85 Å) and the other at high resolution (1.99 Å). Analyzing the crystal contacts of both structures, we concluded that the octameric KtrC-ATP ring is "open" or disrupted (Figure 2C), and a super-helix is formed along a crystallographic axis (Figure 2D). The building blocks of the super-helix are, just like in the octameric rings of KtrA and KtrC, RCK domain dimers. A comparison of the arrangement of the blocks in the two KtrC-ATP structures shows that the super-helices are similar, with only a small deviation in the position of the RCK dimers (Figure S2).

Analysis of the high-resolution KtrC structure shows that, like KtrA and other RCK domains, it is composed by two distinct domains: the N-lobe (residues 3 to 119 from monomer 1 and 120-133 from monomer 2) adopts a Rossmann-fold where the nucleotide binds, and the C-lobe (residues 134 to 218 (Figure 3A)). The two lobes are connected by the α-helix F (αF; residues 120 to 133) that is also involved in domain swapping and dimer formation (Figure 3A). The Root Mean Square Deviation (RMSD) between KtrA-ATP (4J90) or KtrA-ADP (4J91) and KtrC-ATP is 0.92 and 1.35 Å for Cα atoms of the N-lobe, 1.18 and 1.10 Å for Cα of the C-lobe, respectively. A detailed comparison between the high-resolution KtrC and the existing KtrA structures reveals

two structural differences, in the αF helix and in the αC-βD loop (residues 64 to 68). The whole αF helix of KtrC is shifted by ~1.6 Å relative to the same helix in KtrA and the loop is shifted from its position in KtrA, with Cα of Ans66 moved by 4.2 Å (Figure 3B). The proximity between the C terminus of αF helix and of the αC-βD loop suggests that the two structural changes are connected (Figure 3B).

In the high-resolution KtrC-ATP crystal structure, clear electron density is visible for an ATP molecule bound in the nucleotide-binding pocket. ATP assumes an extended conformation similar to the one seen in KtrA, with many of the interacting residues conserved between KtrC and KtrA (Figure 3C). Additionally, a strong electron density peak was observed in the intra-dimer interface, next to the γ-phosphate atom of ATP which is coincidental with a 8σ peak in the anomalous difference electron-density map (Figure 3D). This was interpreted as a calcium ion due to: 1) the presence of 1 mM $CaCl_2$ in the protein solution; 2) the presence of the anomalous-signal peak; and 3) the potentially coordinating atoms surrounding the density peak, two waters, the γ-phosphates of the two ATP molecules and the carboxylic groups of Glu121 from both subunits. Refinement of the Ca^{2+} confirmed the interaction with these chemical groups and shows that the cation bridges the two subunits in the dimer (Figure 3A and 3D). A second calcium ion is present in the inter-dimer interface coordinated by Tyr104 and Gln79 from two subunits (Figure S3); the non-canonical coordination and the lower anomalous density level (4σ) suggest that this is a low-affinity site. It is worthwhile stating that calcium is not a component of the crystallization condition for the low-resolution KtrC-ATP structure, indicating that the super-helical arrangement is not due to the binding of Ca^{2+} to either one of the dimer interfaces. However, we speculate that coordination of Ca^{2+} stabilizes the interfaces and increases the resolution of the diffraction pattern of these crystals.

To understand the structural features that give rise to the super-helical crystallographic arrangement of KtrC-ATP, we need to consider the parameters that define the domain arrangement in the octameric ring. The KtrA-ATP and -ADP octamers, as well as the KtrC-ADP ring structures described above, are arranged with four subunits in a plane and the other four in the plane below, following an up-and-down alternate disposition of subunits around the ring (Figure S4). In these structures the relative positioning of the N-lobes in the RCK domain results from a combination of two angles: the dimer hinge angle, which relates the two subunits in a dimer and is in general identical across all dimers composing a ring (Figure 4A), and the inter-dimer interface angles, which define the relative orientation of two dimers (Figure 4B and 4C). The dimer hinge angle is measured between the αF helices from the two subunits in the dimer; in the KtrC-ATP-Ca^{2+} structure this angle is ~124°, similar to the angle in KtrA-ATP ~120° and wider than in the KtrA-ADP structure ~112° (Figure 4A). The inter-dimer interface angle is measured from the relative orientation of the helices mediating the contact, more specifically from the rotation angle of helices αD and αE in one subunit relative to the same pair of helices in the other subunit, across the contact (Figure 4B and 4C). In KtrA-ATP the inter-dimer interface angle is ~90° for all the contacts; in KtrA-ADP two alternating inter-dimer interfaces are observed which differ in the respective angle, ~90° and ~60°. In KtrC-ATP-Ca^{2+} the angle is ~59°, very similar to one of the angles measured in KtrA-ADP (Figure 4B). This shows that the angles in KtrC are within the range of values observed for KtrA and that the crystallographic organization in KtrC is not the result of unusual contacts between subunits.

To compare the organization of RCK domains in the super-helix and in the rings we generated an eight subunit (four dimers) section of the KtrC-ATP-Ca^{2+} super-helix and superposed it with the KtrA-ADP octameric ring. We matched the N-lobe from one end

of the KtrC helical section with a KtrA-ADP N-lobe which displays an inter-dimer interface angle of ~60º. With this superposition the inter-dimer angles for the superposed subunit are similar in KtrA and KtrC (59º and 60º, respectively) and therefore the two N-lobes across that interface occupy the same volume (Figure 4D). As you go around clockwise along the KtrA ring, the dimer units alternate between the two planes in the ring (Figure S4; Figure 4D). However, the KtrC dimer units start immediately to diverge from these planes (Figure 4D). This divergence results from the specific combination of dimer hinge and inter-dimer angles present in the KtrC-ATP structure that do not allow the dimer units to return back to the planes in the octameric rings.

There is another structural feature that is worthwhile describing, the total surface area buried in the inter-dimer interface of KtrC-ATP (540 $Å^2$) is smaller than in KtrA-ATP (695 $Å^2$). Additionally, the KtrC-ATP-Ca^{2+} contacts involve exclusively Van der Waals interactions, contrasting with some of the KtrA structures deposited in PDB database in which hydrogen bonds and salt bridges are also involved in dimer-to-dimer interactions. In particular, in KtrC an apolar residue (Ile82) replaces one of the residues involved in hydrogen bonding in an inter-dimer interface of KtrA (Thr86).

Interaction between KtrC and KtrD

It has been proposed that the physiological role of KtrC in *B. subtilis* is to regulate the activity of the cation channel KtrD. Our observation that KtrC-ATP in solution exists in multiple oligomeric forms raises the possibility that its interaction with KtrD is different from the one observed for KtrA and KtrB. We investigated the functional and structural relationship between KtrC and KtrD.

We first analyzed the ability of KtrC to form a complex with KtrD. For this, we mixed purified KtrC-ATP with half of a detergent-solubilized cell extract containing KtrD and then pulled-down KtrD from both batches (with and without KtrC) using a His-tag affinity beads. Imidazole eluted KtrD and KtrD-KtrC proteins were then loaded into a size-exclusion chromatography column (Figure 5A). Comparing the elution profiles of the KtrC-KtrD mixture with elution of KtrD alone reveals an extra peak around 9.7 ml, which coincides with the elution volume of the KtrAB complex; SDS-PAGE analysis of the 9.7 ml peak fraction confirms the presence of both proteins, demonstrating assembly of the two proteins in a complex (Figure 5B). Hence, the instability of KtrC-ATP octameric ring does not appear to compromise KtrCD complex formation.

We also used an *in vivo* assay where the ability of KtrC to activate KtrD was assessed by complementation of a growth deficiency in the *Escherichia coli* TK2420 strain. This strain is defective in K^+ uptake systems and growth requires at least 30 mM K^+ in the medium; unless a functional K^+ transporter is expressed, promoting growth at lower K^+ concentrations (Albright et al., 2007; Vieira-Pires et al., 2013). Accordingly, TK2420 cells were transformed with a vector constitutively expressing the KtrC and KtrD proteins together or alone, and growth of these cells was assessed in minimal media with different K^+ concentrations, ranging from 0.03 to 115 mM (Figure 5C). TK2420 cells expressing the two proteins grew well at 6 mM K^+ concentration, contrasting with cells expressing only KtrC or KtrD, that required 30 mM K^+. These results fit well with the idea that KtrC associates with KtrD, generating a functional channel.

We also tested the ability of KtrC to form a functional complex with KtrB using the complementation assay (Figure 5C). The results clearly show that KtrCB rescues the growth phenotype as well as KtrAB. Moreover, KtrA and KtrD also form a functional complex, demonstrating that KtrA and KtrC are functionally redundant. The K^+

requirements of the different complexes, 6 mM for KtrCD and KtrAD and 1 mM for KtrAB and KtrCB show that this is a property of the membrane protein, KtrD or KtrB. This difference can have several explanations; for example, a larger number of KtrB molecules on the membrane relative to KtrD would result in a more effective transport of K^+ into the cell. However, it also fits well with the proposal that a single KtrD channel is less efficient than KtrB in mediating K^+ flux (Holtmann et al., 2003).

Cyclic-di-AMP binding to KtrC

The nucleotide c-di-AMP is an important secondary messenger in many Gram-positive bacteria, including in *B. subtilis* and *S. aureus*, and has been proposed to have a crucial role in K^+ homeostasis (Commichau et al., 2015; Commichau et al., 2018; Gundlach et al., 2018; Gundlach et al., 2017). KtrA from *S. aureus* was identified as binding cyclic-di-AMP (Corrigan et al., 2013; Kim et al., 2015); the same has been proposed for KtrC due to its high sequence similarity with *S. aureus* KtrA (64% protein sequence identity). Thus, we tested whether c-di-AMP and other related molecules bind to KtrC using a thermal shift assay. In this assay, the fluorescence of the Sypro Orange dye increases when it binds to the protein hydrophobic regions that become exposed as the protein is denaturated with increasing temperature (Niesen et al., 2007; Vedadi et al., 2006). Ligand binding generally triggers protein stabilization and an increase in the melting temperature is indicative of an interaction between the small molecule and the macromolecule. We measured an increase of ≥11°C in the melting temperature of KtrC in the presence of c-di-AMP (0.2 mM) (Figure 6A); other structurally related ligands, namely cyclic-AMP, cyclic-di-IMP and cyclic-di-GMP (0.2 mM), did not cause changes in melting temperature ($\Delta T < 1$ °C). Thus, c-di-AMP is a likely ligand of KtrC.

We confirmed c-di-AMP binding to KtrC by Isothermal Titration Calorimetry (ITC) (Figure 6B). Data analysis using a single-site binding model reveals a binding stoichiometry of ~0.5, corresponding to one molecule of c-di-AMP bound to a KtrC-ADP dimer. The binding dissociation constant (K_D) was ~30 nM (K_A= 3.4535 x10^7 ± 1.3306 x10^6 M^{-1}, ΔH = -12286 ± 38 cal mol^{-1}, -TΔS = 2003 ± 44 cal mol^{-1} K^{-1}; values were obtained from global fitting of 3 replicates). The stoichiometry is in agreement with previously published data for the C-lobe of KtrA from *S. aureus* KtrA, strongly suggesting that c-di-AMP binds in the interface of the C-lobes of KtrC (Kim et al., 2015).

We also analyzed the c-di-AMP binding properties of KtrA for comparison. In the thermal shift assay, c-di-AMP increases the melting temperature of KtrA by ~2.5 ºC while c-di-GMP, c-di-IMP and cAMP had a small impact (ΔT < 1 ºC) (Figure 6C). This suggests that c-di-AMP binds to KtrA but that its affinity is lower than for KtrC. Accordingly, ITC experiments with KtrA and c-di-AMP determined a K_D ~3 µM (K_A = 33496 ± 7211 M^{-1}, ΔH= -5796 ± 71 cal mol^{-1} and -TΔS = -1741 ± 72 cal mol^{-1} K^{-1}; values were obtained from global fitting of 4 replicates) with a binding stoichiometry ~0.5 (Figure 6D). As for KtrC, this stoichiometry corresponds to one molecule of c-di-AMP bound to a KtrA dimer.

Considering that KtrC exists in solution as multiple oligomeric species that are dependent on protein concentration and on the bound ligand, ATP or ADP, we wondered if c-di-AMP could also affect the oligomer distribution. We analyzed the impact of c-di-AMP binding on the oligomeric state of KtrC by size-exclusion chromatography. Accordingly, 50 µl at 8 mg/ml of KtrC-ATP and KtrC-ADP were incubated with c-di-AMP (0.2 mM) (Figure 6E) and loaded into the column. The chromatograms clearly show that KtrC in the presence of c-di-AMP elutes as a sharp

454 single peak at approximately 11 ml, without any other peaks detected at higher elution
455 volumes. The elution volume of the peak observed for KtrC with bound c-di-AMP
456 suggests an octamer.

457 Unfortunately, and despite our best efforts, we could not obtain diffracting crystals of
458 KtrC or KtrA with c-di-AMP, either in the presence of ATP or ADP. Beautiful crystals
459 were formed but never diffracted to better than 12 Å. Overall, our data clearly shows
460 that c-di-AMP binds tightly to KtrC, that its affinity for KtrA is 100-fold lower and that
461 this ligand strongly stabilizes the KtrC octamer.

462

Discussion

We have characterized the molecular properties of the KtrC protein and have shown that it adopts different oligomeric states in solution, most likely a tetramer and octamer. Moreover, we have shown that KtrC binds ATP, ADP and c-di-AMP and that these ligands affect the oligomerization state of KtrC. ADP stabilizes the octamer relative to ATP and c-di-AMP strongly stabilizes the octamer. Mg^{2+} also appears to stabilize the octamer, in particular with ATP. Accordingly, crystal structures of KtrC with ADP show an octameric ring while KtrC-ATP forms super-helices that run across the crystal.

The central question underlying this work is, what are the differences in the molecular properties of KtrC relative to KtrA? Our characterization has shown that like KtrA, KtrC binds ATP and ADP, that it forms octamers and that these octamers adopt a ring arrangement. Also like in KtrA, the KtrC octameric rings with bound ADP adopt a non-square conformation which in KtrA corresponds to a low-activity state (Szollosi et al., 2016; Vieira-Pires et al., 2013). We also showed that KtrC and KtrD assemble together in a complex form that has a similar elution volume to that previously observed for KtrAB (Vieira-Pires et al., 2013), suggesting a similar quaternary organization. Moreover, we have demonstrated that KtrA and KtrC have the ability to be functionally interchangeable since they can form functional channels with both KtrB and KtrD.

A striking difference between the two proteins is that, in solution, KtrA has always been observed as an octamer while KtrC with ATP or ADP appears to exist in an equilibrium between octamers and non-octameric species. In KtrC, ADP favors the formation of octamers, relative to ATP. Crystal structures of KtrC with ATP reveal that the KtrC dimeric units assemble as a non-closed oligomer, a super-helix, by establishing inter-dimer contacts that are similar to contacts seen in KtrA. We propose that in the crystallization conditions, with high precipitant and protein concentrations, the KtrC-

ATP non-octameric species favor the establishment of inter-dimer contacts that result in the formation of the super-helix.

Our high-resolution ATP structure also shows the presence of Ca^{2+} in the intra-dimer and inter-dimer interfaces. Particularly interesting is the site in the intra-dimer interface where the divalent cation bridges residues and ATP phosphate groups from two subunits. In addition, our solution characterization revealed that Mg^{2+} slightly stabilizes the octameric species in the presence of ATP. Other RCK domains are known to bind nucleotides and divalent cations; in particular, the RCK domain of the GsuK channel has been crystallized with AMP and Ca^{2+} and it has been shown that these two ligands affect channel function (Kong et al., 2012). Altogether, this suggests that divalent cations have a structural and functional role in KtrC.

Why are KtrC octamers less stable than in KtrA? We can think of two possibilities: 1) the smaller buried surface area and the contacts established in the inter-dimer interface, in particular the lack of hydrogen bonding, result in weaker interfaces; 2) the distribution of conformations available to KtrC dimers, resulting from the combination of dimer hinge angle and inter-dimer angle, is different from KtrA and results in lower stability of the octameric ring assembly. We prefer the second explanation over the first because c-di-AMP binding strongly stabilizes the formation of octamers in solution. Others have shown that c-di-AMP binds in the interface between the RCK C-lobes and our measured value for stoichiometry fits well with this model (Kim et al., 2015). In KtrC this binding site is more than 50 Å away from the inter-dimer interface, making c-di-AMP induced conformational changes in the protein regions mediating the inter-dimer contacts unlikely (Figure 7A). However, the arrangement of the C-lobes has been shown to be altered upon c-di-AMP binding. A comparison of the structures of the C-lobe in KtrC with that of the C-lobe bound to c-di-AMP from its orthologue in *S. aureus*

shows a rotational rigid body movement of the lobes upon ligand binding. This change results in a ~4 Å increase in the distance separating equivalent residues positioned close to the αF helix (Figure 7A and 7B). As the C-lobes are directly linked to the αF helices, it is likely that upon c-di-AMP binding the C-lobe rearrangement will be propagated to the dimer hinge angle affecting the spatial relationship of the N-lobes in the dimer, altering the distribution of inter-dimer and intra-dimer angles and stabilizing a dimeric unit conformation that favors the formation of a KtrC octameric ring. A similar rigid-body mechanism also explains how binding of ATP or ADP to the site in the N-lobe (close to the intra-dimer interface) impacts the stability of the octamer.

We have also demonstrated that c-di-AMP interacts tightly with KtrC while it binds to KtrA with 100-fold lower affinity. c-di-AMP is an important signaling molecule in *B. subtilis* where it has been proposed to be a major regulator of K^+ homeostasis. It was previously shown that c-di-AMP binds to the KtrC ortholog *in S. aureus* and proposed that the ligand inhibits K^+ flux (Bai et al., 2014; Commichau and Stulke, 2018; Zeden et al., 2018). The binding affinity measured by us for KtrC and this ligand, together with the physiological concentrations of c-di-AMP in the cytosol of *B. subtilis* (2-5 µM) (Oppenheimer-Shaanan et al., 2011), would imply that in the cell, KtrC is saturated with inhibiting ligand. However, it is possible that within the context of the fully assembled KtrCD complex the affinity is lower, possibly bringing it to a physiological range. The similarities between Ktr proteins in *S. aureus* and those studied here suggest that c-di-AMP will also inactivate the Ktr channels from *B. subtilis*.

In conclusion, despite strong amino acid sequence similarity, KtrC and KtrA display different molecular properties, in particular in oligomerization and c-di-AMP binding. Further studies will be required to fully understand the functional and physiological impact of these differences and to know if these properties are further modulated by

other cytosolic factors. Nevertheless, we can speculate that the ability of KtrC to form different oligomeric assemblies and its dependence on ATP, ADP and c-di-AMP serves specific roles in the cell.

Acknowledgments

We thank the technical support provided by the i3S scientific platform “Biochemical and Biophysical Technologies” and access to synchrotron Soleil (PROXIMA 1 and 2A) for collection of X-ray diffraction data.

Funding

Work was supported by *Fundação Luso-Americana para o Desenvolvimento* through the FLAD Life Science 2020 award entitled “Bacterial K^+ transporters are potential antimicrobial targets: mechanisms of transport and regulation” and by FEDER - Fundo Europeu de Desenvolvimento Regional funds through the COMPETE 2020 - Operacional Programme for Competitiveness and Internationalisation (POCI), Portugal 2020, and by Portuguese funds through FCT - Fundação para a Ciência e a Tecnologia/Ministério da Ciência, Tecnologia e Ensino Superior in the framework of the project POCI-01-0145-FEDER-029863 (PTDC/BIA-BQM/29863/2017) and of project "Institute for Research and Innovation in Health Sciences" (POCI-01-0145-FEDER-007274). RR was supported by FCT fellowship (SFRH/BPD/111525/2015), CMT-D was supported by FCT fellowship (SFRH/BD/123761/2016).

References

Adams, P.D., Grosse-Kunstleve, R.W., Hung, L.W., Ioerger, T.R., McCoy, A.J., Moriarty, N.W., Read, R.J., Sacchettini, J.C., Sauter, N.K., Terwilliger, T.C., 2002. PHENIX: building new software for automated crystallographic structure determination. Acta Crystallogr. D: Biol. Crystallogr. 58, 1948-1954.

Albright, R.A., Joh, K., Morais-Cabral, J.H., 2007. Probing the structure of the dimeric KtrB membrane protein. J. Biol. Chem. 282, 35046-35055.

Albright, R.A., Ibar, J.L., Kim, C.U., Gruner, S.M., Morais-Cabral, J.H., 2006. The RCK domain of the KtrAB K+ transporter: multiple conformations of an octameric ring. Cell 126, 1147-1159.

Bai, Y., Yang, J., Zarrella, T.M., Zhang, Y., Metzger, D.W., Bai, G., 2014. Cyclic di-AMP impairs potassium uptake mediated by a cyclic di-AMP binding protein in Streptococcus pneumoniae. J. Bacteriol. 196, 614-623.

Bakker, E.P., Mangerich, W.E., 1981. Interconversion of components of the bacterial proton motive force by electrogenic potassium transport. J. Bacteriol. 147, 820-826.

Cao, Y., Pan, Y., Huang, H., Jin, X., Levin, E.J., Kloss, B., Zhou, M., 2013. Gating of the TrkH ion channel by its associated RCK protein TrkA. Nature 496, 317-322.

Commichau, F.M., Stulke, J., 2018. Coping with an Essential Poison: a Genetic Suppressor Analysis Corroborates a Key Function of c-di-AMP in Controlling

578 Potassium Ion Homeostasis in Gram-Positive Bacteria. J. Bacteriol. 200,
579 e00166-00118.

580 Commichau, F.M., Dickmanns, A., Gundlach, J., Ficner, R., Stulke, J., 2015. A jack of
581 all trades: the multiple roles of the unique essential second messenger cyclic di-
582 AMP. Mol. Microbiol. 97, 189-204.

583 Commichau, F.M., Gibhardt, J., Halbedel, S., Gundlach, J., Stulke, J., 2018. A Delicate
584 Connection: c-di-AMP Affects Cell Integrity by Controlling Osmolyte
585 Transport. Trends Microbiol. 26, 175-185.

586 Corratge-Faillie, C., Jabnoune, M., Zimmermann, S., Very, A.A., Fizames, C.,
587 Sentenac, H., 2010. Potassium and sodium transport in non-animal cells: the
588 Trk/Ktr/HKT transporter family. Cell. Mol. Life Sci. 67, 2511-2532.

589 Corrigan, R.M., Campeotto, I., Jeganathan, T., Roelofs, K.G., Lee, V.T., Grundling, A.,
590 2013. Systematic identification of conserved bacterial c-di-AMP receptor
591 proteins. Proc. Natl. Acad. Sci. USA 110, 9084-9089.

592 Diskowski, M., Mikusevic, V., Stock, C., Hanelt, I., 2015. Functional diversity of the
593 superfamily of K(+) transporters to meet various requirements. Biol. Chem. 396,
594 1003-1014.

595 Diskowski, M., Mehdipour, A.R., Wunnicke, D., Mills, D.J., Mikusevic, V., Bärland,
596 N., Hoffmann, J., Morgner, N., Steinhoff, H.-J., Hummer, G., Vonck, J., Hänelt,

I., 2017. Helical jackknives control the gates of the double-pore K(+) uptake system KtrAB. Elife 6, e24303.

Dong, J., Shi, N., Berke, I., Chen, L., Jiang, Y., 2005. Structures of the MthK RCK domain and the effect of Ca2+ on gating ring stability. J. Biol. Chem. 280, 41716-41724.

Dumas, P., Ennifar, E., Da Veiga, C., Bec, G., Palau, W., Di Primo, C., Pineiro, A., Sabin, J., Munoz, E., Rial, J., 2016. Extending ITC to Kinetics with kinITC. Methods Enzymol. 567, 157-180.

Epstein, W., Schultz, S.G., 1965. Cation Transport in Escherichia coli: V. Regulation of cation content. J. Gen. Physiol. 49, 221-234.

Grundling, A., 2013. Potassium uptake systems in Staphylococcus aureus: new stories about ancient systems. MBio 4, e00784-00713.

Gundlach, J., Commichau, F.M., Stulke, J., 2018. Perspective of ions and messengers: an intricate link between potassium, glutamate, and cyclic di-AMP. Curr. Genet. 64, 191-195.

Gundlach, J., Herzberg, C., Kaever, V., Gunka, K., Hoffmann, T., Weiss, M., Gibhardt, J., Thurmer, A., Hertel, D., Daniel, R., Bremer, E., Commichau, F.M., Stulke, J., 2017. Control of potassium homeostasis is an essential function of the second messenger cyclic di-AMP in Bacillus subtilis. Sci. Signal 10, eaal3011.

Harley, C.A., Jesus, C.S., Carvalho, R., Brito, R.M., Morais-Cabral, J.H., 2012. Changes in channel trafficking and protein stability caused by LQT2 mutations in the PAS domain of the HERG channel. PLoS One 7, e32654.

Hite, R.K., MacKinnon, R., 2017. Structural Titration of Slo2.2, a Na(+)-Dependent K(+) Channel. Cell 168, 390-399.

Hite, R.K., Yuan, P., Li, Z., Hsuing, Y., Walz, T., MacKinnon, R., 2015. Cryo-electron microscopy structure of the Slo2.2 Na(+)-activated K(+) channel. Nature 527, 198-203.

Holtmann, G., Bakker, E.P., Uozumi, N., Bremer, E., 2003. KtrAB and KtrCD: two K+ uptake systems in Bacillus subtilis and their role in adaptation to hypertonicity. J. Bacteriol. 185, 1289-1298.

Jiang, Y., Pico, A., Cadene, M., Chait, B.T., MacKinnon, R., 2001. Structure of the RCK domain from the E. coli K+ channel and demonstration of its presence in the human BK channel. Neuron 29, 593-601.

Jiang, Y., Lee, A., Chen, J., Cadene, M., Chait, B.T., MacKinnon, R., 2002. Crystal structure and mechanism of a calcium-gated potassium channel. Nature 417, 515-522.

Kim, H., Youn, S.J., Kim, S.O., Ko, J., Lee, J.O., Choi, B.S., 2015. Structural Studies of Potassium Transport Protein KtrA Regulator of Conductance of K+ (RCK) C

635 Domain in Complex with Cyclic Diadenosine Monophosphate (c-di-AMP). J.
636 Biol. Chem. 290, 16393-16402.

637 Kong, C., Zeng, W., Ye, S., Chen, L., Sauer, D.B., Lam, Y., Derebe, M.G., Jiang, Y.,
638 2012. Distinct gating mechanisms revealed by the structures of a multi-ligand
639 gated K(+) channel. Elife 1, e00184.

640 Kroll, R.G., Booth, I.R., 1981. The role of potassium transport in the generation of a pH
641 gradient in Escherichia coli. Biochem. J. 198, 691-698.

642 Leonetti, M.D., Yuan, P., Hsiung, Y., Mackinnon, R., 2012. Functional and structural
643 analysis of the human SLO3 pH- and voltage-gated K+ channel. Proc. Natl.
644 Acad. Sci. USA 109, 19274-19279.

645 Levin, E.J., Zhou, M., 2014. Recent progress on the structure and function of the
646 TrkH/KtrB ion channel. Curr. Opin. Struct. Biol. 27C, 95-101.

647 Meury, J., Robin, A., Monnier-Champeix, P., 1985. Turgor-controlled K+ fluxes and
648 their pathways in Escherichia coli. Eur. J. Biochem. 151, 613-619.

649 Niesen, F.H., Berglund, H., Vedadi, M., 2007. The use of differential scanning
650 fluorimetry to detect ligand interactions that promote protein stability. Nat.
651 Protoc. 2, 2212-2221.

652 Oppenheimer-Shaanan, Y., Wexselblatt, E., Katzhendler, J., Yavin, E., Ben-Yehuda, S.,
653 2011. c-di-AMP reports DNA integrity during sporulation in Bacillus subtilis.
654 EMBO Rep. 12, 594-601.

655 Price-Whelan, A., Poon, C.K., Benson, M.A., Eidem, T.T., Roux, C.M., Boyd, J.M.,
656 Dunman, P.M., Torres, V.J., Krulwich, T.A., 2013. Transcriptional profiling of
657 Staphylococcus aureus during growth in 2 M NaCl leads to clarification of
658 physiological roles for Kdp and Ktr K+ uptake systems. MBio 4, e00407-00413.

659 Roosild, T.P., Miller, S., Booth, I.R., Choe, S., 2002. A mechanism of regulating
660 transmembrane potassium flux through a ligand-mediated conformational
661 switch. Cell 109, 781-791.

662 Roosild, T.P., Castronovo, S., Miller, S., Li, C., Rasmussen, T., Bartlett, W.,
663 Gunasekera, B., Choe, S., Booth, I.R., 2009. KTN (RCK) domains regulate K+
664 channels and transporters by controlling the dimer-hinge conformation.
665 Structure 17, 893-903.

666 Szollosi, A., Vieira-Pires, R.S., Teixeira-Duarte, C.M., Rocha, R., Morais-Cabral, J.H.,
667 2016. Dissecting the Molecular Mechanism of Nucleotide-Dependent Activation
668 of the KtrAB K+ Transporter. PLoS Biol. 14, e1002356.

669 Vedadi, M., Niesen, F.H., Allali-Hassani, A., Fedorov, O.Y., Finerty, P.J., Jr., Wasney,
670 G.A., Yeung, R., Arrowsmith, C., Ball, L.J., Berglund, H., Hui, R., Marsden,
671 B.D., Nordlund, P., Sundstrom, M., Weigelt, J., Edwards, A.M., 2006. Chemical
672 screening methods to identify ligands that promote protein stability, protein

673 crystallization, and structure determination. Proc. Natl. Acad. Sci. USA 103,
674 15835-15840.

675 Vieira-Pires, R.S., Szollosi, A., Morais-Cabral, J.H., 2013. The structure of the KtrAB
676 potassium transporter. Nature 496, 323-328.

677 Whatmore, A.M., Reed, R.H., 1990. Determination of turgor pressure in Bacillus
678 subtilis: a possible role for K+ in turgor regulation. J. Gen. Microbiol. 136,
679 2521-2526.

680 Winn, M.D., Ballard, C.C., Cowtan, K.D., Dodson, E.J., Emsley, P., Evans, P.R.,
681 Keegan, R.M., Krissinel, E.B., Leslie, A.G., McCoy, A., McNicholas, S.J.,
682 Murshudov, G.N., Pannu, N.S., Potterton, E.A., Powell, H.R., Read, R.J., Vagin,
683 A., Wilson, K.S., 2011. Overview of the CCP4 suite and current developments.
684 Acta Crystallogr. D: Biol. Crystallogr. 67, 235-242.

685 Wu, Y., Yang, Y., Ye, S., Jiang, Y., 2010. Structure of the gating ring from the human
686 large-conductance Ca(2+)-gated K(+) channel. Nature 466, 393-397.

687 Ye, S., Li, Y., Chen, L., Jiang, Y., 2006. Crystal structures of a ligand-free MthK gating
688 ring: insights into the ligand gating mechanism of K+ channels. Cell 126, 1161-
689 1173.

690 Yuan, P., Leonetti, M.D., Pico, A.R., Hsiung, Y., MacKinnon, R., 2010. Structure of the
691 human BK channel Ca2+-activation apparatus at 3.0 A resolution. Science 329,
692 182-186.

693 Zeden, M.S., Schuster, C.F., Bowman, L., Zhong, Q., Williams, H.D., Grundling, A.,
694 2018. Cyclic di-adenosine monophosphate (c-di-AMP) is required for osmotic
695 regulation in Staphylococcus aureus but dispensable for viability in anaerobic
696 conditions. J. Biol. Chem. 293, 3180-3200.

697

698

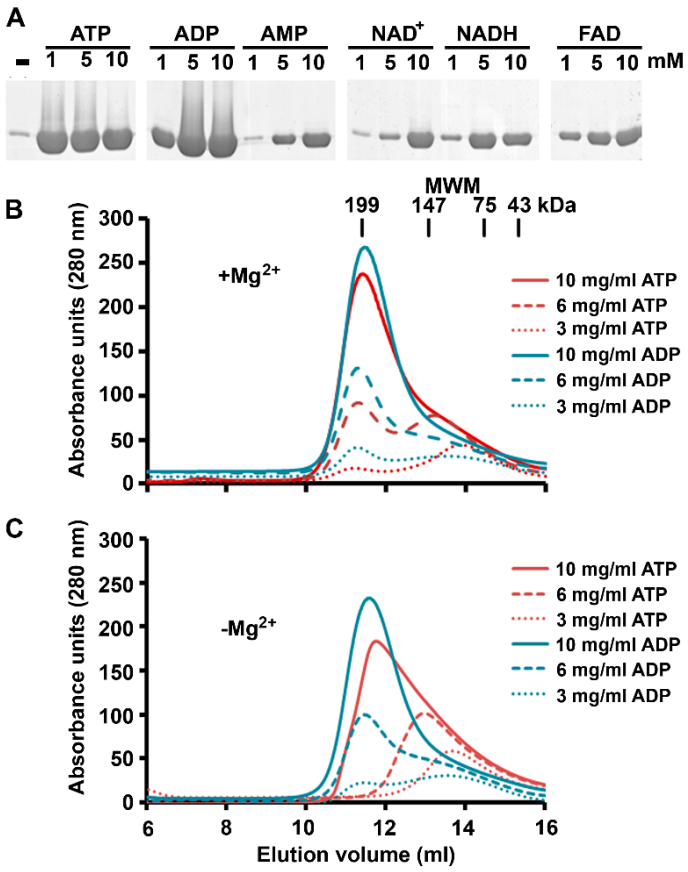

Figure 1. KtrC binds ATP and ADP. A) SDS-PAGE of KtrC eluted from ADP-agarose beads with 1, 5 and 10 mM of indicated adenosine nucleotides. **B)** Size-exclusion elution profile of KtrC-ATP and KtrC-ADP at 10, 6 and 3 mg/ml. Protein samples were loaded in a Superdex 200 column (GE Healthcare) in the presence of $MgCl_2$ and elution profiles were monitored by absorption at 280 nm. Elution volumes of *B. subtilis* KtrA (199 kDa), yeast alcohol dehydrogenase (147 kDa), chicken egg white Conalbumin (75 kDa) and hen egg Ovalbumin (43 kDa) are shown. **C)** As in B) but without $MgCl_2$ in the sample and elution buffers.

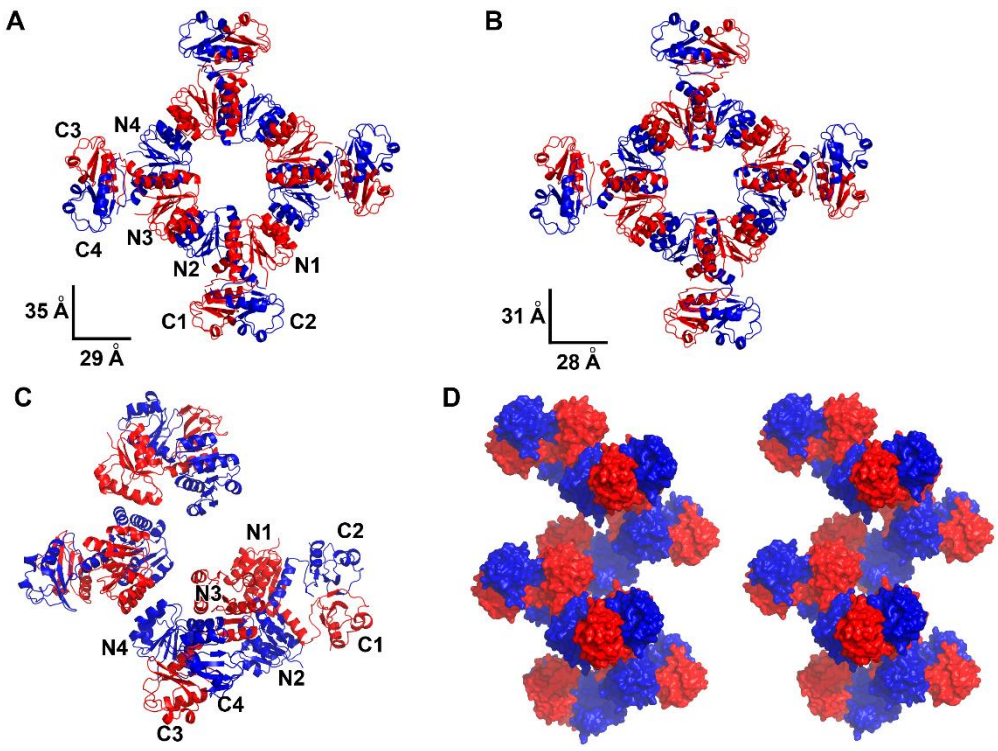

Figure 2. KtrC crystal structures. Cartoon representations of the KtrC-ADP crystal structures determined at **A)** 5.69 Å (space group $P6_222$) and **B)** 6.28 Å (space group $P2_1$) showing octameric rings in a non-square conformation. Subunits are colored in red and blue; N and C lobes of some subunits are labeled. Dimensions of ring hole are based on distances measured between Asp34 Cα in subunits positioned across the ring. **C)** Cartoon representation of an octamer in the crystal of KtrC-ATP-Ca^{2+} at 1.99 Å showing an open ring. N and C lobes of some subunits are labeled. **D)** Stereo-view of several asymmetric units of the KtrC-ATP-Ca^{2+} crystal, evidencing a super-helix.

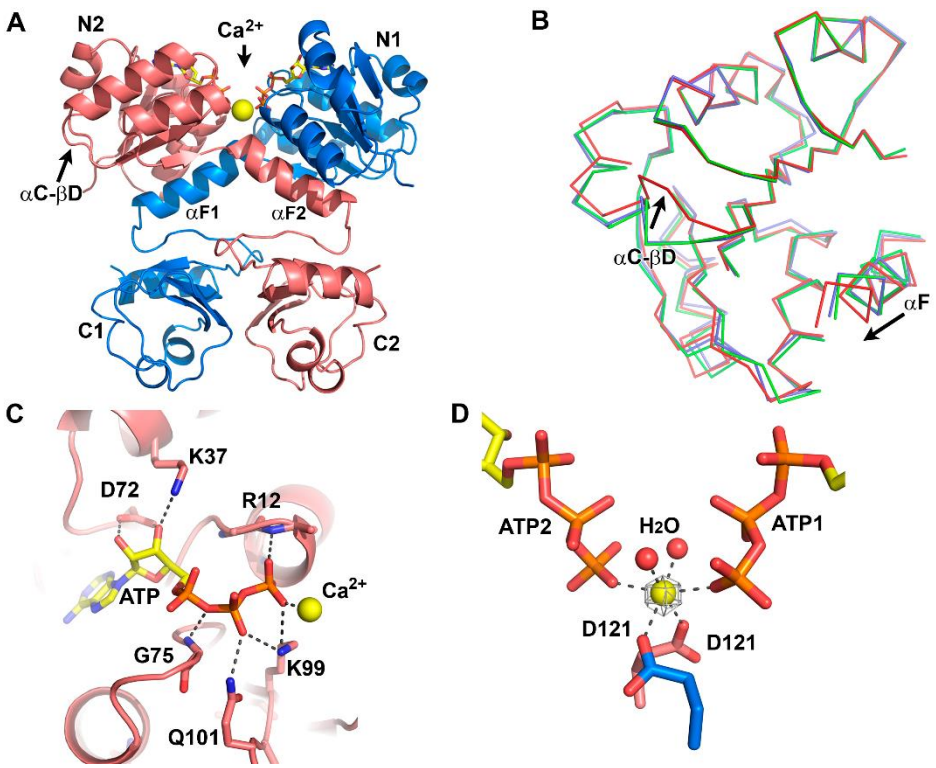

Figure 3. KtrC-ATP-Ca^{2+} structure. A) Cartoon representation of KtrC-ATP-Ca^{2+} homodimer. ATP molecules are shown in yellow stick. A calcium ion is shown as yellow sphere. N and C lobes are labeled. α-helices involved in domain swapping (αF) and αC-βD loop are indicated. **B)** Cα trace superposition of N-terminal domains (residues 1 to 119) from KtrC-ATP-Ca^{2+} (red), KtrA-ATP (blue; PDB code 4J90) and KtrA-ADP (green; PDB code 4J91). Two structural alterations are observed in KtrC-ATP-Ca^{2+} in comparison with KtrA structures: shift of the αF and movement of αC-βD loop. **C)** ATP binding site with some of the ligand interactions shown as dashed lines and residues labeled. **D)** Close-up view of Ca^{2+} coordination in the intra-dimer interface. Ca^{2+} is hexa-coordinated with two waters and carboxylic groups in Glu121 (one from each subunit) in the same plane and oxygen atoms of ATP γ-phosphate in the axial positions. Anomalous-signal difference map for calcium is represented as gray mesh (contour 5.0 σ).

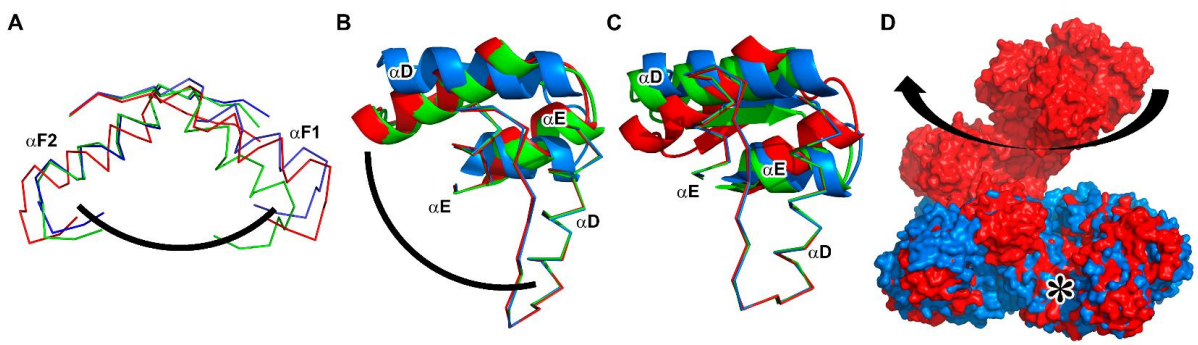

Figure 4. Details of super-helical arrangement in KtrC-ATP-Ca^{2+}. A) Intra-dimer hinge angle measured between αF helices in KtrC-ATP-Ca^{2+} (red), KtrA-ATP (blue; PDB code 4J90) and KtrA-ADP (green; PDB code 4J91). Structures were superimposed by residues in a single N-lobe, excluding αF. Dimer hinge angle is indicated by arc and is approximately 124° in KtrC-ATP-Ca^{2+}, 120° in KtrA-ATP and 112° in KtrA-ADP. **B)** and **C)** Inter-dimer contact superposition. αD and αE helices from two interacting subunits in KtrC-ATP-Ca^{2+} (red) and KtrA-ATP (blue) superposed with the two different contacts observed in KtrA-ADP (green). The αD and αE helices from the subunits above the plane of figure were superimposed and represented as a line; αD and αE helices in the opposing subunit are represented as cartoon. The inter-dimer interface angle is indicated by arc and relates one pair of helices with the other across the interface. **D)** Superposition of KtrC-ATP-Ca^{2+} octamer (colored in red) and KtrA-ADP octamer (colored in blue). Star indicates N-lobe used for superposition; arrow shows the clockwise direction along which the position of the RCK dimers diverge in the two structures.

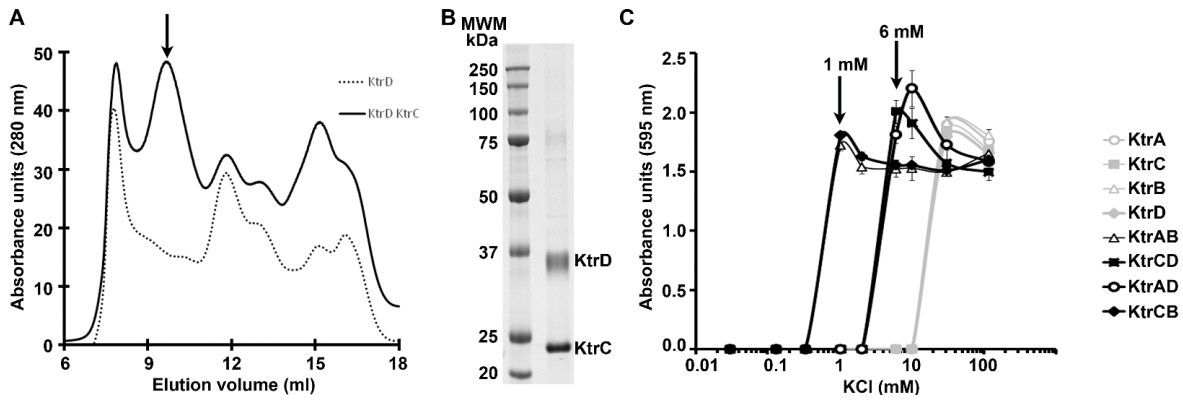

Figure 5. Functional and biochemical assembly of KtrCD. A) Size-exclusion profiles of KtrD-KtrC mixture and of KtrD alone. Peak containing KtrCD complex (elution volume ~9.7 ml) is indicated by arrow. **B)** SDS-PAGE analysis of fraction from elution peak corresponding to KtrCD complex. Two proteins are visible: KtrC (24.3 kDa) and KtrD (49.4 kDa). The membrane protein migrates below its molecular weight. **D**) Functional complementation assay. Cell density of *E. coli* TK2420 cultures expressing the various combinations of RCK domain proteins (KtrC and KtrA) with membrane proteins (KtrB and KtrD) or expressing a single protein alone, grown under different K^+ concentrations. Minimal K^+ concentrations at which phenotype complementation occurs are indicated.

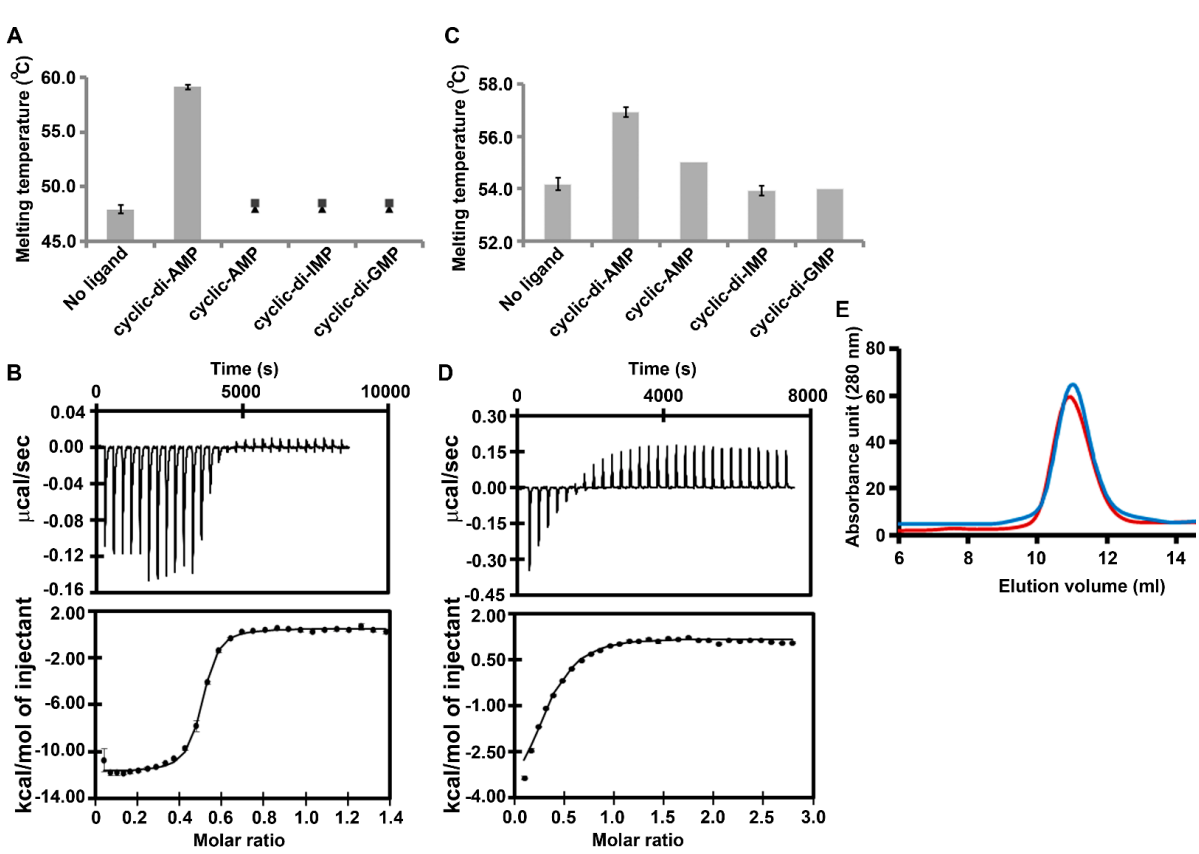

Figure 6. Cyclic-di-AMP binding. A) Plot of melting temperatures of KtrC without ligand and with 200 µM of indicated ligand. For conditions without ligand and with c-di-AMP mean ± standard deviation is shown, (n=4). For other nucleotides only two measurements were performed and the individual values are plotted. **B)** Representative plot of ITC experiment of KtrC (10 µM) titrated with cyclic-di-AMP (72 µM) in the presence of 5 mM $MgCl_2$. Upper graph shows heat power changes during titrations. Lower graph shows integrated heat values fitted with binding model. **C)** Plot of melting temperatures of KtrA without ligand and with 250 µM of indicated ligand. Mean ± standard deviation is shown, (n=6); for the two conditions where error bar is not visible the 6 replicates gave identical results. **D)** Representative plot of ITC experiment of KtrA (30 µM) titrated with cyclic-di-AMP (400 µM) in the presence of 5 mM $MgCl_2$. Panels as in A). **E**) Representative chromatograms of size-exclusion profiles of KtrC-ATP-

Mg^{2+} (red) and KtrC-ADP-Mg^{2+} (blue) incubated with 0.2 mM c-di-AMP. Running buffer had no Mg^{2+}.

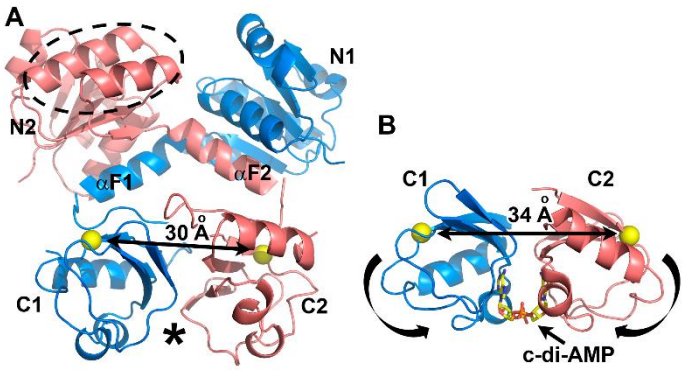

Figure 7. Structures of KtrC from *B. subtilis* and of C-lobe from Ktr orthologue in *S. aureus*. A) Cartoon representation of KtrC dimer. Valine153 (Cα) is shown as yellow sphere in both subunits, with distance separating the atoms indicated. N and C lobes are labeled. KtrC region involved in the inter-dimer contact is indicated by dashed oval. Putative binding site of c-di-AMP is marked by star. **B)** Cartoon representation of structure of C-lobe from *S. aureus* KtrA bound to cyclic-di-AMP (PDB code 4XTT). c-di-AMP is indicated. Cα of residues equivalent to KtrC Val153 are shown as yellow spheres; distance separating atoms is shown. Curved arrows indicate the possible movement of the C-lobes upon ligand binding, as concluded from comparison of structures in A) and B). Cα r.m.s.d. between KtrC-ATP and KtrAΔN-lobe is 1.07 Å.